Multimodal laser-based angioscopy for structural, chemical and biological imaging of atherosclerosis

Luis E. Savastano[1,*], **Quan Zhou**[2], **Arlene Smith**[2], **Karla Vega**[3], **Carlos Murga-Zamalloa**[4], **David Gordon**[4], **Jon McHugh**[4], **Lili Zhao**[5], **Michael Wang**[6,7], **Aditya Pandey**[1], **B. Gregory Thompson**[1], **Jie Xu**[8], **Jifeng Zhang**[8], **Y. Eugene Chen**[8], **Eric J. Seibel**[3], and **Thomas D. Wang**[2,9,10]

[1]Department of Neurosurgery, University of Michigan, Ann Arbor, MI, USA

[2]Department of Biomedical Engineering, University of Michigan, Ann Arbor, MI, USA

[3]Department of Mechanical Engineering, University of Washington, Seattle, WA, USA

[4]Department of Pathology, University of Michigan, Ann Arbor, MI, USA

[5]University of Michigan School of Public Health, Ann Arbor, MI, USA

[6]Department of Neurology, University of Michigan, Ann Arbor, MI, USA

[7]VA Ann Arbor Healthcare System, Ann Arbor, MI 48105, USA

[8]Center for Advanced Models and Translational Sciences and Therapeutics, University of Michigan Medical School, 2800 Plymouth Road, Ann Arbor, MI 48109-2800, USA

[9]Division of Gastroenterology, Depar. of Medicine, University of Michigan, Ann Arbor, MI

[10]Department of Mechanical Engineering, University of Michigan, Ann Arbor, MI, USA

Abstract

The complex nature of atherosclerosis demands high-resolution approaches to identify subtle thrombogenic lesions and define the risk of plaque rupture. Here, we report the proof-of-concept use of a multimodal scanning fiber endoscope (SFE) consisting of a single optical fiber scanned by a piezoelectric drive that illuminates tissue with red, blue, and green laser beams, and digitally reconstructs images at 30 Hz with high resolution and large fields-of-view. By combining laser-

CORRESPONDENCE: Luis E. Savastano, MD, Department of Neurosurgery, University of Michigan, 1500 E. Medical Center Drive, Room 3552 TC, Ann Arbor, MI 48109-5338, Phone: 734-647-7960; Fax: 734-936-9294, lsavasta@med.umich.edu.
ADDITIONAL INFORMATION/CORRESPONDING AUTHOR: Luis E. Savastano, MD, Department of Neurosurgery, University of Michigan, 1500 E. Medical Center Drive, Room 3552 TC, Ann Arbor, MI 48109-5338, Phone: 734-647-7960; Fax: 734-936-9294, lsavasta@med.umich.edu

induced reflectance and fluorescence emission of intrinsic fluorescent constituents in arterial tissues, the SFE allowed us to co-generate endoscopic videos with a label-free biochemical map to derive a morphological and spectral classifier capable of discriminating early, intermediate, advanced, and complicated atherosclerotic plaques. We demonstrate the capability of scanning fiber angioscopy for the molecular imaging of vulnerable atherosclerosis by targeting proteolytic activity with a fluorescent probe activated by matrix metalloproteinases. We also show that the SFE generates high-quality spectral images *in vivo* in an animal model with medium-sized arteries. Multimodal laser-based angioscopy could become a platform for the diagnosis, prognosis, and image-guided therapy of atherosclerosis.

Cardiovascular disease is the main cause of morbidity and mortality worldwide and it is predominantly caused by atherosclerosis. Historically, atherosclerosis has been viewed as a disease of uncontrolled plaque growth causing symptoms when a critical degree of stenosis occurs[1,2]. However, recent insights into atherosclerosis biology have demonstrated that pathological changes within the vessel wall, rather than degree of stenosis, determine the fate of a plaque[3,4]. Currently, rupture of the attenuated fibrous cap of an inflamed atherosclerotic plaque is considered to be the most common precipitating factor that culminates in thrombosis and ischemia[5,6–8]. Despite improved understanding of the structural and biological factors that makes plaques rupture prone and symptomatic, conventional non-invasive diagnostic modalities used in the workup of carotid and coronary atherosclerotic disease continue to be primarily employed for stenosis quantification and detection of macroscopic changes in the vessel wall[9]. These techniques are optimal from a clinical screening standpoint, but the complex nature of atherosclerosis often demands higher resolution approaches to detect thromboembolic lesions and define the potential risk for future rupture[7,9–12]. In the last two decades, new intravascular modalities have emerged for intraluminal imaging of atherosclerosis, such as endovascular endoscopy, or angioscopy, intravascular ultrasound, optical coherence tomography, and optical spectroscopy methods. However, a stand-alone platform capable of generating real-time structural, chemical, and biological images of large vascular surfaces to reveal high-definition pathological hallmarks of vulnerable and complicated atherosclerotic lesions, both for diagnostic and prognostic purposes and to guide intraluminal interventions, is still an unmet clinical need[13,14].

Here, we demonstrate the use of a multimodal endoscope technology to collect laser-induced reflectance and fluorescence simultaneously and perform structural and biological evaluation of atherosclerosis. We use these co-registered images to generate a classifier to stage the extent of disease with histological corroboration. Our approach for scanning fiber angioscopy (SFA) is based on the scanning fiber endoscope (SFE). This system consists of an ultrathin, highly flexible catheter that scans blue, green, and red laser beams (wavelengths are 424, 488, and 642 nm) in a spiral pattern on the tissue surface, and collects reflectance and fluorescence (from extrinsic or intrinsic fluorophores) through a ring of optical fibers (Fig. 1)[15]. Then, multimodal images are reconstructed in real time with a large field-of-view (FOV) and projected with high spatial resolution of ~12 μm at typical imaging distances (equivalent to 200,000 to 250,000 pixels). By combining reflectance and laser-induced fluorescence emission of intrinsic fluorescent constituents in vascular tissue, we were able to co-generate endoscopic videos with label-free biochemical makeup of healthy and diseased

arteries. We employed this multimodal information to derive a morphological and spectral classifier capable of discriminating early, intermediate, advanced, and complicated plaques. We also demonstrated that the superior image resolution of this technology revealed intravascular thrombi and surface thrombogenic lesions, even in cases not detected by conventional diagnostic modalities. Then, by targeting proteolytic activity of complicated atherosclerotic plaques with a fluorescence agent activated by matrix metalloproteinases (MMPs), we were able to identify vulnerable regions of weakened fibrous cap at a resolution far beyond clinically available technology[16]. Finally, as a prelude for clinical use, we demonstrate feasibility by performing *in vivo* spectral angioscopy in a medium-sized animal model. Multimodal laser-based angioscopy holds the potential to become a powerful platform for research, diagnosis, prognosis, and image-guided local therapy in atherosclerosis and cardiovascular disease.

RESULTS

In order to evaluate the ability of the multimodal SFE to distinguish normal from abnormal endovascular surfaces, to classify lesions throughout the pathological spectrum of atherosclerosis, and reveal the hallmarks of complicated lesions, we started by analyzing a set of carotid arteries harvested at autopsy. Please refer to the Online Methods section and Supplementary Fig. 1–5 for a detailed description of material and methods. We obtained multimodal SFE videos (Supplementary Videos 1–5) with mean area of ~50 cm^2 of the endoluminal surface (average radius of carotid 3mm; average length 100 mm)[17] from a composite of a total of 22 fresh carotid arteries and 1 vertebral artery, and compared the findings to "gold-standard" endoscopic images obtained with a white-light endoscope. Of all the lesions encountered, we selected 29 for blinded histological correlation (10 initial xanthoma, 5 pathological intimal thickening, 6 atheroma, 5 ulcerated plaque, 2 intraluminal thrombus) that were matched to 20 representative "healthy" endovascular surfaces (11 specimens) for histological correlation (Supplementary Table 1). The SFE system consistently generated high-resolution, wide-field images equivalent to ~200,000 pixels of 360° (ie, entire circumference) of the luminal surface of all the specimens analyzed, with diameters ranging from 25mm (at the level of the carotid bifurcation [CB]) to 3mm (vertebral artery). SFE videos, merging high anatomical definition from light reflectance and chemical contrast from tissue fluorescence, were generated at 30 Hz without the need to regulate focus or correct for working distance, which varied from 2 to 20 mm. Laser intensity was adjusted as needed: 1) decreased in very short working distances to avoid light saturation; 2) increased in long working distances to optimize signal from the distant tissues. Per our pre-defined protocol, the handheld SFE was advanced or pulled back at approximately 1cm/sec during image acquisition. Therefore, the SFE generated videos at a rate of 2.5 cm^2 of the vascular surface per sec that resulted in the entire adult carotid artery with proximal internal and external branches scanned in 10 seconds. We analyzed each specimen at least twice with the same channels and laser settings and reliably found analogous images from the same vascular segments, verifying performance of this technology.

In order to improve characterization, analysis, and interpretation of laser-induced tissue fluorescence, fluorescence emission of representative samples (n=5) of tunica media (TM),

fibrous cap, necrotic core, and thrombus from arterial walls were collected via fiber-coupled spectrophotometer (Fig. 1c–h and Table 1). Excitation at 424 nm consistently generated strong blue fluorescence from the TM (453.7±36.5), followed by the necrotic core (336.3±26.4), and then fibrous cap (237.8±18.2) with an intensity drop to 74% and 52%, respectively (Fig. 1f). Negligible fluorescence signal (16.2±1.9) was collected from the thrombus (only 3.57% of the intensity registered from the TM). A similar pattern of green autofluorescence (AF) was observed with 488 nm excitation, but with proportionally reduced intensity peaks (Fig. 1g). Negligible red fluorescence was detected with the 642nm laser in any of the constituents analyzed (Fig. 1h).

This dual modality (fluorescence/reflectance) facilitated navigation of the instrument and optimized recognition of architectural features of early, intermediate, and advanced atherosclerotic lesions. It also revealed the pathological hallmarks of complicated atherosclerotic lesions, even in cases not detected by conventional diagnostic modalities (Table 2). Statistical analysis of target-to-background (T/B) fluorescence log ratios and test agreement can be found in Supplementary Tables 1–3. *Ex vivo* spectral video angioscopy of healthy and diseased human carotid arteries with representative atherosclerotic lesions can be found in Supplementary Videos 1 to 5; *in vivo* spectral video angioscopy in a medium-size animal model can be found in Supplementary Video 6.

SFA of normal carotid arteries

In specimens harvested from subjects without risk factors for atherosclerosis (n=3), SFA revealed delicate smooth endoluminal surfaces with homogeneous reflectance and intense blue and green AF (Fig. 2a–g and Supplementary Video 1). Average normalized signal intensity of distance-compensated fluorescence images (Supplementary Fig. 1) was 73.52 (SD 23.59). No red fluorescence was observed. Microscopic analysis of arterial cross-section showed normal arterial histology [ie, tunica intima (TI), TM, and tunica externa/adventitia (TE)] (Fig. 2h). Confocal microscopy revealed intense blue and green fluorescence originating from elastin in the internal elastic lamina and TM, in comparison with the lower signal background from the collagen matrix. No red AF was observed with the confocal microscopy at 642 nm excitation. Pathological analysis of "normal" regions per multimodal SFE occasionally revealed a scattered proliferation of smooth muscle cells underlying the intima, in a proteoglycan rich matrix with occasional scarce macrophages (Table 2). These subtle findings, corresponding to intimal thickening, were not readily distinguished by endoscopy and were included under the "normal" category for statistical analysis (Table 2, Supplementary Tables 1–3).

SFA of early atherosclerotic lesion

In specimens harvested from donors with minor risk factors for atherosclerosis, SFA revealed raised dot-like or streak-like endoluminal lesions, with macroscopically discrete borders from the surrounding vascular wall, clustered at the CB and origin of the internal carotid artery (ICA). Excitation of vascular surfaces with green and blue lasers revealed minor attenuation of AF signal from the lesions compared to the surrounding vascular surface (Fig. 2i–n and Supplementary Video 2). Distance-compensated T/B ratios were 0.6 on average (SD 0.21), with an estimated log ratio of –0.57 (SE 0.21). Histological analysis

of these lesions revealed focal accumulations of fat-laden macrophages in a thickened intima consistent with initial xanthomata (Fig. 2o). Confocal microscopy revealed lower fluorescence intensity from the focal accumulations of fat-laden macrophages and thickened intima in comparison with the strong signal of elastin in the TM (Fig. 2p).

SFA of intermediate atherosclerotic lesion

In specimens obtained from subjects with risk factors for atherosclerosis, large elevated lesions were observed with white light and SFE reflectance (Fig. 3a,b and Supplementary Video 3). These lesions, clustered in the CB, had lower green and blue AF in comparison with the surrounding endoluminal surface secondary to the reduced fluorescence peak intensity from the lipidic components (Fig. 3b–f). Distance-compensated T/B ratio was 0.43 on average (SD 0.17) with an estimated log ratio of −0.91 (standard error [SE] 0.31). Cross-sectional microscopic histology revealed multiple layers of fat-laden macrophages at the intima with sparse free-lipid deposits in the deep portion of the lesions and no distinct fibrous cap layer of connective tissue separating the lesion from the vascular lumen (Fig. 3g). Confocal microscopy confirmed very low AF derived from the intermediate atheroma compared to the intense blue and green AF originating from elastin in the TM (Fig. 3h).

SFA of advanced atherosclerotic lesion

In patients with strong risk factors for and/or history of carotid atherosclerotic disease, large lesions protruding into the vascular lumen or causing circumferential stenosis were identified in the CB and in the proximal ICA side (Fig. 3i). These lesions had ill-defined borders and appeared smooth and homogeneous on reflectance. Blue and green channels consistently revealed low AF even in non-protruding or stenosing lesions, in comparison with the surrounding endoluminal surface (Fig. 3j–l and Supplementary Video 4). The reduced fluorescence from these lesions was likely secondary to specific fluorochromes in the plaques with lower emission capacity than elastin and by attenuating the excitation of autofluorochromes in the TM (ie, like a superimposed filter). Distance-compensated T/B ratio was 0.44 on average (SD 0.18), with an estimated log ratio of −0.92 (SE 0.28). Histological analysis of these lesions revealed fibrous cap atheroma characterized by a thick layer of smooth muscle cells in a collagenous proteoglycan matrix covering a lipid or necrotic core (Fig. 3m). Reduction of luminal AF detected by SFE in fibroatheromas correlated with an increase in thickness of the fibrous cap, which frequently caused positive remodeling of the vessel. Fluorescence analysis with confocal microscopy revealed a thick-capsule fibroatheroma with low blue and green AF interposed between the vascular lumen and the TM (Fig. 3m). This differential chemical contrast was instrumental for rapid identification of advanced atherosclerotic lesions not causing significant luminal stenosis even in vascular segments that would appear normal by white-light systems or SFE reflectance surface anatomy (Supplementary Fig. 2).

SFA of complicated atherosclerotic lesion

Intraplaque hemorrhage—A subset of advanced atherosclerotic lesions was found to have distinct areas within the plaque domes that were reddish-brown colored on white-light system (Fig. 4a). These distinct regions within advanced plaques had dark gray areas of low

reflectance associated with negligible AF (Fig. 4b–f and Supplementary Video 5). Histological analysis revealed intraplaque hemorrhage (Fig. 4a), likely explaining the poor AF secondary to the high extinction coefficient of hemoglobin. The intraplaque hemorrhage had negligible AF per confocal microscopy. The outstanding sensitivity of the SFE technology to demonstrate hemoglobin-dependent light extinction can be further appreciated in Supplementary Fig. 3.

Ulcerated plaque—In specimens harvested from donors with known artery-to-artery embolic strokes, we identified shallow punched-out lesions with raised irregular borders (Fig. 4k–t). These lesions had a central portion of subtle reddish-brown color on the white-light system and a darker gray color in SFE reflectance secondary to low-light reflectance (Fig. 4g–h and Supplementary Video 5). Blue and green laser excitation of these lesions provoked a distinctive speckled pattern characterized by multiple irregular dots of strong AF in a background of very low AF (Fig. 4k–m). This chemical contrast, especially prominent in the blue channel, had a distance-compensated T/B ratio (necrotic debris as target, crater of ulcer as background) of 5.34 on average (SD 5), with an estimated log ratio of 1.33 (SE 0.31). Ulcerated plaque was the only pathological category with an estimated log ratio >0, or normalized ratio >1 ($p=0.0007$) (Supplementary Table 2). Histological analysis of these "starry sky" regions revealed disruption of fibrous cap with exposure of lipidic necrotic material to the lumen (Fig. 4n). Confocal microscopy showed highly heterogeneous AF signal from the necrotic core mingling with thrombus exposed in the crater of the ulcerated plaque to the vascular lumen. The spectral speckled pattern was exclusively identified in ulcerated plaques in this study.

Intraluminal thrombus—These are subocclusive or occlusive intraluminal lesions with variable reflectance (based on age of thrombus) and very low AF (Fig. 4o–y). In this study, chronic thrombi with ongoing organization and deposition of connective tissue had near normal reflectance with light gray appearance and minimal AF (Fig. 4r–u). Instead, acute thrombi had negligible reflectance and AF likely secondary to a higher hemoglobin concentration, and were identified as black or dark gray intraluminal lesions (Fig. 4v–y). These chemical contrasts from laser-induced florescence were confirmed by confocal microscopy of arterial cross-sections.

Test agreement between multimodal SFE, pathology diagnoses

By combining the above-mentioned structural information with label-free chemical contrast into a classifier and blindly assigning 29 lesions to specific diagnostic groups, we found near-perfect agreement (kappa=0.998; 95% CI 0.964–1.000) with weighted Kappa statistics between multimodal SFE diagnosis and pathologic diagnosis by conventional histological techniques (kappa of 0, no agreement; kappa of 1, complete agreement) (Supplementary Table 3). The single error found in 49 assessments adjudicated an initial xanthoma to the intermediate lesion group of SFA, likely secondary to the limited cross-section resolution of SFE technology.

SFA of proteolytic activity of atherosclerotic lesion

After testing the power of the multimodal SFE to detect and characterize atherosclerotic lesions based on structural and spectral features, we explored the capability of this platform to target biological markers of plaque vulnerability. We imaged the proteolytic activity in the fibrous cap of human symptomatic atherosclerotic lesions by detecting fluorescence from activated MMPSense 645 Fast. This imaging agent is optically silent before activation and emits intense fluorescence (excitation 649 nm, emission 666 nm) after cleavage by a range of MMPs highly expressed in vulnerable atherosclerotic plaques[18]. After institutional approval, we collected three endarterectomy specimens removed at surgery from patients that recently suffered strokes secondary to artery-to-artery emboli from complicated carotid plaques (Fig. 5a–c). Macroscopic inspection revealed ulcerated plaques, one of them associated with a large intraluminal thrombus (Fig. 5d,o). The SFE revealed homogeneous reflectance and delicate blue and green AF from the fibrous cap, with negligible AF from the IT (Fig. 5e–f). No AF was observed with the red channel, which was confirmed by scanning the specimen with a sensitive fluorescence detector (Fig. g,h). After incubation with the activatable imaging agent, intense fluorescence preferentially distributed in the area of the fibrous cap associated with the IT was observed with the red channel of the SFE (Fig. 5i,j). In our samples of symptomatic lesions, the abluminal surface (ie, away from the lumen toward the outer surface of the artery) of the plaques also expressed MMP signals, although had no defined distribution pattern and was significantly weaker than the signal detected in the endoluminal surface (average radiance $p/s/cm^2/sr$ of 5.08E+09 endoluminal vs 1.86E+09 abluminal; Fig. 5m,n). MMPSense-generated fluorescence was replicated with conventional confocal microscopy and point-spectrometer analysis, which revealed a fluorescence emission peak at 666nm for activated MMPSense 645 and optical silence for inactive MMPSense 645 (Fig. 5k,l). *In situ* zymography confirmed the presence of active MMP in corresponding areas with red fluorescence signal identified by the SFE after MMPSense incubation (Fig. 5o).

In vivo multimodal SFA in infrarenal aorta of rabbit

In vivo endovascular endoscopy of the infrarenal aortoiliac vessels was performed in New Zealand rabbits with a 1.2mm SFA. Using the reverse Seldinger technique, the right common carotid artery was accessed and a 7F sheath was placed and connected to continuous heparinized saline solution (Fig. 6a–c). Then, a 6F+ cello balloon guide catheter was navigated into the infrarenal abdominal aorta under roadmap assistance and connected to heparinized flush. At this point, the SFA was advanced in coaxial fashion and a clear FOV was obtained by anterograde blood flow interruption via balloon insufflation and saline flush (Fig. 6d–f). High-resolution multimodal angioscopic images of the whole vessel circumference were generated at 30Hz (Supplementary Video 6). Although the aortic diameter ranged from 3 to 6 mm, there was no need to regulate focus or correct for working distance. Aortas of the living animals had delicate, smooth homogenous endoluminal surfaces in reflectance with strong blue autofluorescence, which was corroborated with confocal fluorescence microscopy after vessel harvesting (Fig. 6g–h). In our experience, small amounts of intraluminal blood, generally entering the vessels in a retrograde fashion by collateral branches, obscured FOV of the angioscope. The latter was addressed after balloon insufflation by continuous heparinized saline solution flush, adjusted as needed from

30 to 50 mL/min (note intraluminal blood compromising image quality in the first 5 seconds of Supplementary Video 6, seconds 00:09 to 00:14, that clears after increasing saline flush).

DISCUSSION

Non-invasive imaging platforms have had tremendous growth over the past decade and enabled new insight into atherosclerosis biology and vascular wall structure[14,16]. However, the complex spatiotemporal nature and heterogeneity of atherosclerotic lesions within and between individuals often demands higher resolution approaches that are provided by noninvasive imaging to define the potential risk of future cardiovascular events and identify thrombogenic lesions in complicated plaques[19,20]. To date, angioscopy is considered the most precise clinical diagnostic tool to identify thrombogenic lesions and intravascular thrombus in coronary arteries and to monitor in real-time the apposition of stent struts to the arterial wall[21–25]. Fiberoptic angioscopes, received with great enthusiasm in the 1980's, were also combined with different band-pass and band-absorption filters for fluorescence imaging to improve *in vivo* characterization of intraluminal thrombi and distinguish some biochemical component of atherosclerotic plaques, such us low-density lipoprotein[26]. Despite advances in manufacturing techniques that increased the number of pixels from 3,000 to 10,000, the image quality remains poor and the system is unable to detect with enough sensitivity fluorescent signal from molecular probes targeting specific biological pathways. In addition, the excessive stiffness of these fiber bundle angioscopes significantly limited their usefulness and applicability in clinical practice[27]. The endoscopic system introduced here, mounted in an ultrathin, highly flexible catheter, consistently generates high-resolution videos with large depth of focus of the entire arterial circumference with simultaneous biochemical contrast from laser-induced fluorescence. The latter phenomenon is based on the presence of intrinsic fluorochromes within healthy and diseased vessels, and can be elicited by low-power laser light sources similar to that used in the SFE. The same optical properties are employed in fluorescence spectrometry, which is a well-established technique to analyze atherosclerotic plaques based on subtle differences in spectral decomposition of arterial fluorochromes[28,29]. This latter technology, however, has not seen significant use in the clinic, given the need for optical contact to couple light collection, the constraints of generating data from pinpoint areas, and the inability to provide structural information of the tissues analyzed[30].

The SFE is a powerful technology that merges high definition angioscopy from diffuse reflectance, label-free chemical contrast from laser-induced AF, and hemoglobin-related light extinction. Multimodal videos are generated in real time from the entire FOV of the endoscope at a resolution far greater than the standard ($\approx$25 times higher), and can therefore provide immediate information to guide management and assist intraluminal therapy. The SFE has front viewing optics to provide a large depth of field and wide FOV to generate sharp remote imaging of vascular surfaces without the need for approaching or crossing potentially unstable atherosclerotic lesions, which could result in plaque rupture and thrombosis. These are major advantages of the SFE for atherosclerosis imaging compared to cross-sectional viewing intravascular imaging devices, such as ultrasound and optical coherence tomography, which depend on lesion proximity and automated rotational pullbacks (ie, crossing unstable lesions back and forth) to reconstruct images of vascular

segments after post-imaging processing[31–33]. In addition, high-degree stenosis or total luminal occlusion precludes the use of lateral-view instruments, which also perform poorly in arterial bifurcations where plaques are overwhelmingly concentrated in carotid arteries and represent 15–20% of coronary lesions[34,35]. For example, the large ulcer at the carotid flow divider clearly demonstrated in Fig. 4g–j would have been extremely challenging, if possible at all, to appropriately image with a lateral-view device such as OCT. Bifurcation plaques are associated with lower procedural success rates and higher long-term adverse event rates during percutaneous coronary interventions compared with non-bifurcation lesions, largely due to suboptimal stent apposition to the vascular wall[36]. The SFE generates videos with large depth of field and wide FOV from a front-view approach, and can therefore guide in real-time mechanical interventions such as thrombectomy in totally occluded arteries and deployment of stents in tortuous anatomy, observe the apposition of the stent struts to the vascular wall or the relationship with other jailing stents in bifurcating vessels, and monitor the vascular surface for complications of mechanical therapy such us dissections or displacement of plaque material into the vascular lumen or branching vessels[37].

Here, we introduce a classification system based on multimodal structural images with chemical contrast that is able to accurately classify atherosclerotic plaques in early, intermediate, advanced, and complicated lesions. We also appropriately discriminate acute from chronic thrombus based on hemoglobin-related light extinction in reflectance mode, which could provide insight into selecting the most efficient reperfusion treatment approach[38]. While the present results are promising, future *in vivo* studies are warranted to determine if hemoglobin is a reliable negative contrast agent in spectral angioscopy. In our study, the SFE was found to be especially powerful in identifying surface defects in complicated plaques, even in cases not detected during routine stroke work up[39]. Therefore, this diagnostic modality could enable the detection of small intravascular thrombi and subtle thrombogenic lesions in a subpopulation of patients with cryptogenic strokes secondary to thromboembolic phenomena from low-grade (<50%) carotid stenosis[39]. In addition, we demonstrated that SFA can be used as a powerful platform for molecular imaging of atherosclerosis vulnerability[40,41]. Arterial lumen occlusion and thromboembolic events are considered acute events driven by disruption of a weakened fibrous cap due to high proteolytic activity[6–8,42]. By targeting proteolytic activity of complicated atherosclerotic plaques with a fluorescence agent activated by MMPs, we were able to identify regions of the fibrous cap associated with rupture with outstanding topographic correlation. The "endoluminal view" of angioscopy offered unsurpassed details of biologically unstable regions within the complex geography of a plaque, and with a resolution far beyond non-invasive technology. Therefore, in addition to the diagnostic/prognostic value of risk of rupture, SFA could guide local therapy for atherosclerosis to the most vulnerable regions.[19] In this regard, it is important to mention that despite improved understanding of atherosclerosis pathophysiology and major advancements in imaging modalities, we have yet to identify which structural and biological features are useful for guiding management and preventing cardiovascular accidents. New multimodality intravascular imaging technology, some of them combining exogenous and endogenous fluorescence detection with OCT or IVUS in the same catheter, are currently being used in humans and hold the

potential to provide better insight into vulnerable and symptomatic atherosclerotic lesions[43–45]. Further research is needed to elucidate the association of high-risk plaque characteristics and clinical events, and to demonstrate that detection and preventive treatment of vulnerable plaques has clinical benefit[46].

In our experiments, we found significant differences in signal intensity and topographical distribution of activated molecular imaging agents from the abluminal and endoluminal surfaces of complicated atheromas (Fig. 5)[47]. Even within the endoluminal area of a single plaque, fluorescence signal from activated probe was mainly confined to the ruptured portion of the fibrous cap associated with the IT. These findings raise the question whether non-invasive diagnostic modalities used for biological imaging of carotid atherosclerosis— although ideal for screening purposes—have the necessary sensitivity and spatial resolution to detect key topographical differences of MMP activity[13,18].

As a prelude to clinical translation, we demonstrated the feasibility of multimodal SFA for *in vivo* endovascular endoscopy in an animal model with medium-sized arteries. Our data confirms that the SFA can be easily navigated in the aorta of these animals and generates high-quality spectral images of the 360° luminal surface with large FOV and depth of view without the need to regulate focus or correct for working distance. In addition, we showed that a clear FOV can be consistently accomplished by stopping anterograde blood flow by inflating a balloon and flushing distally the stagnated blood with crystalloid solution. This blood-free environment can then be efficiently sustained by flushing low volumes of clear solution, both in animal research and in clinical settings as previously shown[23,37]. Based on the rapid image acquisition, it is feasible that SFE angioscopy could occur simultaneously to contrast injection, as clinically done in coronary OCT[48]. In addition, multimodal SFE images are generated with long depth of focus (>5 cm) at 30 times/second, and therefore this technology can give all the information required during a very brief clearing if appropriately positioned by angiography, unlike lateral-view devices that depend on rotational pullbacks throughout a sustained clear FOV. Further research to optimize the endovascular technique for obstructive and non-obstructive (ie, without balloon insufflation) multimodal angioscopy needs to be conducted.

In this study, rather than analyzing subtle differences in spectral decomposition of pinpoint areas through sophisticated algorithms in an attempt to predict the chemical composition of plaques, we deliberately elected to employ major differences in laser-induced AF intensities of the structural components of normal and diseased arteries to complement anatomical images. In addition to facilitating plaque staging, the capability of the SFE system to dissect the biochemical makeup of the major structural components of atherosclerotic lesions and differentiate diseased from normal vascular wall holds the potential to optimize photoablation technology in cardiovascular disease. Laser atherectomy is a debulking strategy employed to open totally occluded vascular lumens from plaques and thrombi, facilitate angioplasty in complex lesions otherwise unsuitable for endovascular therapy, and treat stent re-stenosis[49]. This ablative approach, although conceptually superior to angioplasty that "pushes" the plaque outward to reconstitute a lumen, is associated with a high risk of vessel perforation, given the inability of the laser to discriminate a lesion from the normal arterial wall[50,51]. We have shown that TM of diseased arteries have a much

stronger laser-generated AF signal compared to the overlying atherosclerotic plaques[52]. This laser-induced chemical contrast can be precisely quantified by the SFE with very high temporal and spatial resolution. Therefore, the SFE could selectively deliver targeted photoablation to diseased areas based on AF levels while the beam is following its pre-determined spiral trajectory[53,54,15]. This targeted ablation could continue into the depths of a lesion while respecting normal vascular surfaces by modulating laser intensities, and stop when the fluorescence signal monitored by the SFE reaches a pre-established threshold for "elastin." Therefore, the ability to recognize the TM by laser-induced fluorescence could serve as feedback to more accurately control laser atherectomy[55]. This "smart" technology could minimize healthy vessel wall damage (ie, TM) while maximizing plaque and clot debulking, resulting in a significant reduction in the risk of mural perforation and post-procedural re-stenosis. Feedback-controlled ablation would therefore improve the efficacy and safety profile of laser-based atherectomy, which is especially needed in small tortuous vessels such us the coronary arteries and the cerebral circulation[56]. The possibility offered by SFE technology to deliver guided therapy based on high-resolution multimodal imaging acquired with the same device could be a major gain compared to other catheter-based imaging platforms.

Translation of the SFE into the interventional neurovascular clinic faces many challenges, which were not addressed in this limited *ex vivo* study. The classification system introduced here is intended to discriminate the spectrum of atherosclerotic lesions derived from *ex vivo* analysis of human samples and needs to be corroborated and validated in clinical settings. The latter especially holds true for advanced and complicated plaques, which are most relevant from a clinical management standpoint. Currently, stand-alone SFE provides limited information on the vertical structure of tissues. A combination of SFE with cross-sectional imaging technology, such as OCT, will allow further characterization of different types of fibroatheroma and precise quantification of fibrous cap thickness. Similar to the vast majority of intravascular optical devices, a blood-free vascular segment is required for SFE image acquisition. Classically, this is achieved by proximal balloon insufflation followed by gentle saline flushing when needed. The SFE system being introduced here is able to generate multimodal images from whole human carotid arteries and the major bifurcating branches in 10 seconds and is easily speeded up by >2x (<5 seconds). Therefore, image acquisition could be synchronized to radiopaque (but optically lucent) contrast injection for digital subtraction angiography. A second clinical requirement is the ability to navigate the SFE to the vascular segment, which is often constricted and made more torturous due to disease. Recent SFE designs have a reduced rigid tip length from 9mm to 6mm, and overall diameter from 1.2mm to 0.85mm, and will be used as a disposable device. Additional clinical and regulatory challenges include the ability to fluorescently label luminal walls in human arterial vessels.

Finally, SFE angioscopy has inherent risks due to the invasive nature of this approach, which must be considered at the time of clinical use. Carotid arteries are generally large straight vessels with pathology concentrated at the bifurcation, and are routinely catheterized for diagnostic purposes with a 0.03% risk of asymptomatic embolic events using modern endovascular techniques[57]. Therefore, they represent the most logical and safe target for first-inhuman use of intravascular SFE in its current dimension. In this regard, the forward-

viewing approach of SFE with its large depth of field provides an edge on safety for invasive imaging of vulnerable and complicated atherosclerosis compared to lateral-view technology such as IVUS and OCT. If a lesion looks vulnerable to dislodge, then the SFE can provide this diagnosis without blindly passing across the lesion and risking damage that would be unrecorded, and potentially catastrophic, if imaging requires movement of the scope across the lesion first. If additional information is needed, such as imaging the backside, then the SFE can be advanced across the lesion after assessing the situation proximally.

In this paper, we introduce the first intra-arterial forward-viewing device capable of generating real-time structural, chemical, and biological images of large vascular surfaces at a resolution far greater than the standard. By synergistically combining high-definition endovascular endoscopy, laser-generated fluorescence, and molecular imaging of key biological processes, this catheter-based technology holds the potential to become a new platform for research, diagnosis, prognosis, and image-guided local therapy in atherosclerosis and cardiovascular disease.

ONLINE METHODS

The medical branch of our research team consists of 3 cerebrovascular neurosurgeons (including the first author of the manuscript) and 1 stroke neurologist. We treat patients affected by stroke due to intra- and extra-cranial atherosclerosis on a daily basis. The clinical need of detecting high-risk and symptomatic lesions in carotid and vertebral arteries was the driving force to conduct this study. The carotid endarterectomy samples and the cohort of arteries analyzed in this study included specimens obtained from patients treated by our medical team after suffering artery-to-artery stroke, such as the case in Fig. 4 that presents an ulcerated plaque in cryptogenic stroke and a vertebral artery with acute-on-chronic intraluminal thrombus complicated by stroke.

Specimens

Following institutional approval, 22 carotid arteries and 1 vertebral artery were harvested from hospital autopsies of 22 adult human cadavers without known history of trauma, head and neck surgery, or neuroendovascular procedure. Autopsy donors included patients with: 1) no risk factors for atherosclerosis; 2) major risk factors for atherosclerosis (eg, high blood pressure, tobacco use, diabetes, high blood fat levels, family history, age, obesity, and sedentarism) or documented asymptomatic carotid atherosclerotic disease; 3) stroke secondary to artery-to-artery embolism from ruptured plaque; or 4) history of cryptogenic (unknown) stroke[58]. Specimens were freed from surrounding connective tissue, and cleaned and preserved moist with saline solution until image acquisition, which was performed immediately after harvesting. Of these samples, the first 5 specimens harvested were employed for fiber-coupled fluorescence spectrometry and for exploratory multimodal angioscopy. These specimens were then processed for histology and analyzed by an unblinded pathologist. The data obtained from these 5 specimens was employed to construct a multimodal classifier for atherosclerosis (see below). The remaining 18 specimens in the cohort were imaged with multimodal laser angioscopy, processed for histology, and selected lesions were independently reviewed by pathologists and matched to endoscopic images. In

addition, 3 atherosclerotic plaques removed during carotid endarterectomy surgery from patients that suffered ipsilateral stroke within the previous 2 weeks were collected and maintained moist with saline solution at 4 °C until image acquisition performed within 12hrs. Macroscopic photos of all specimens were obtained with Canon PowerShot G16 Digital Camera. Informed consent was obtained from all subjects.

Multispectral SFE

This experimental forward-viewing fluorescence imaging system consists of a single optical fiber that is scanned by a piezoelectric drive mechanism to illuminate tissue surface with red, blue, and green laser beams (RGB) in an outwardly expanding spiral pattern[15]. Reflectance is collected by a ring of step-indexed plastic optical fibers and then digitalized to reconstruct a two-dimensional color video image from the entire FOV of the endoscope, with a full cone angle in air of 70–100 degrees, and in water (or a saline solution such us normal saline) of 60–90 degrees[15]. However, unlike conventional color video, the RGB color channels are imaging laser-induced fluorescence for detecting fluorescence species in the tissues for chemical contrast. A fourth channel is used to generate anatomical tissue contrast from red reflectance, which creates a grayscale image. Thus, high-quality, laser-based, fluorescence video imaging with large fields-of-view can be collected from extensive surfaces for research and clinical applications. The images have a spatial resolution of ~12 at typical imaging distances. The depth of view is >50mm using 2.1mm scopes with highest amounts of light collection efficiency. The 1.2mm scope probes have the same spatial resolution as the larger 2.1mm scope, since the resolution is defined for the focused laser beam interacting with the tissue. However, the 1.2mm scope probes have a smaller diameter ring of collection optical fibers surrounding the same laser-based fiber scanner, thus producing lower signal levels so the contrast at longer distances from the scope tip can go down into the noise floor before the larger 2.1mm scope probe[15].

This system is depicted in Fig. 1 and the four imaging channels are B-fluorescence (470/28nm), G-fluorescence (531/46nm), R-fluorescence (>647nm), and grayscale reflectance at 642nm. Yang et al. 2014, report *in vitro* test results from initial validation of the multispectral SFE system with sensitivity limits set for high-contrast video-rate imaging[59]. The endoscopic probe of the SFE system is highly flexible, can be custom-made at different lengths (our system is ≈1.5 meters long), and the optical system can be mounted in a 1.2mm or 2.1mm cross-section diameter shaft. A system with very similar mechanical properties and sizes was recently shown to be safely and effectively navigated in the vascular tree within a coaxial catheter system in a translational animal model[37]. The laser power coming out of the distal tip of the endoscope is <2 mW for each channel, a level consistent with a non-significant risk (NSR) determination by the United States Food and Drug Administration (FDA, 21 CFR 812) for future human clinical studies.

Fiber-coupled fluorescence spectrometry

In order to improve characterization, analysis, and interpretation of SFE laser-induced tissue fluorescence, intrinsic fluorescence (AF) emission of representative samples of TM (mainly formed by elastin and collagen) (*n*=5), fibrous cap (FC; collagen fibers and smooth muscle cells), necrotic core (NC; heterogeneous mix of extracellular matrices and lipids, mainly

cholesterol esters phospholipids), and thrombus (T; mix of red blood cells, platelets, and fibrin) from healthy and diseased arterial walls were collected with a fiber-coupled spectrophotometer (Ocean Optics, Inc., Dunedin, FL)[28]. Fluorescence emission measurements were serially performed after excitation with a diode-pumped solid state laser with λex = 424nm, 488nm, and 642nm. These laser excitation wavelengths match the lasers used with the SFE. AF spectra may also be taken with the SFE *in vivo* at the center of the image when the scanning fiber is stationary, ie, between video frames[60]. The average spectra were plotted with GraphPad Prism software (Graphpad Software, Inc., La Jolla, CA). To avoid signal contamination, representative tissues were mechanically isolated and consecutive specimen sections processed for histological validation.

Multimodal SFE video acquisition of post-mortem arteries

Endoluminal endoscopic videos (Supplementary Videos 1–5) and still images were obtained by navigating the SFE probe into the common carotid artery (CCA) toward the CB and then into the first 2cm of the ICA and external carotid artery (ECA). Images were obtained under normal saline solution, and room light dimmed to avoid light contamination. To achieve concurrent dual-mode SFE color imaging, the green laser was turned off while the blue laser-excited blue fluorescence was imaged, or the blue laser was turned off to image green laser-excited fluorescence. The anatomical details of the luminal wall were recorded in grayscale using red reflectance in all cases. In order to confirm the consistency of this technology to provide equivalent endoscopic images from the same vascular segments, we scanned each specimen at least twice, maintaining the same laser and acquisition settings. The 2.1mm scope was employed for multimodal imaging in all specimens except for the vertebral artery that was imaged with the 1.2mm scope, given the small luminal size over-imposed with a sub-occlusive thrombus.

Quantification of SFE fluorescence

A new method developed in this study is the ability to provide quantitative high-contrast AF-reflectance (dual-mode) imaging using this multispectral SFE. A previously developed method to compensate for fluorescence signal variation from variable distances between the SFE scope tip and luminal wall was applied post-processing, but has also been implemented in real-time video (this distance-compensation algorithm is fully explained and validated *in vitro* by Yang et al., 2013)[61]. For example, the dual-mode SFE image of weak AF far down in the lumen is compensated to be greater due to weak signal recovery from the reflectance signal. Thus, equal AF looking down the lumen will show more even color contrast in the dual-mode SFE image after the distance-compensation algorithm is applied. Otherwise, the central parts of the luminal image will always look darker, even if the concentration of fluorescence species in the luminal wall is uniform, such as in a normal artery.

This step allows pixel intensities to be quantified and is particularly useful for detecting lesions at large angles[62]. Once distance-compensation is applied, the original and distance-compensated fluorescence images are color mapped (high to low maps of colors X to Y) to allow for easy comparison (Supplementary Fig. 1). A line scan displaying intensity value per pixel across this line of pixels is taken at different radial distances to further analyze fluorescence. The T/B ratio is computed along the line scan (circular or straight) by using

random small square areas (four pixels per side) in the target region versus the background region. A minimum of 10 random square areas are taken as the target and 10 as the background to compute the T/B ratio. The software also allows for expert selection of target and background areas. In specimens with no targetable lesion by multimodal SFA, 10 random square areas were selected from the vascular surface at the level of the CB (0cm) and at +1cm, +3cm and +5cm (from the CB toward the CCA), and at −1cm (from the CB toward the ECA and ICA) (Supplementary Fig. 4d). Analysis of variance (ANOVA) model was used to compare fluorescence log-transformed ratios between different pathology diagnoses (if log ratio=0, then ratio=1) (Supplementary Tables 1, 2). The model includes a random effect to consider the correlation between lesions within the same patient. All analyses were conducted using SAS software, version 9.4 (SAS Institute, Cary, NC).

Multimodal analysis of endoluminal images

Endovascular endoscopic videos were reviewed and the surface anatomy described by contour (flat, elevated, excavated, or punched-out), texture (smooth or ragged), presence of surface defect or thrombus, reflectance in grayscale, and AF signal in blue, green, and red colors, surface patterns (homogeneous or speckled), and T/B ratio. SFE images were compared with images obtained with a high-definition pediatric cysto-urethroscope (Storz endoscope; Karl Storz Endoscopy-America, Inc., El Segundo, CA). This commercially available white-light system is mounted on a 11.5cm rigid shaft with an outer diameter of 9.5F (3.17mm). Surface anatomy by SFE was combined with label-free chemical contrast provided by fluorescence quantifications as described above.

Based on our previous experience with arterial surface architecture and laser-induced AF signal generated by multimodal endovascular SFE, and an extensive literature review on angioscopic appearance of carotid atherosclerotic disease[22,24,63], we created an endoscopic classification scheme to correlate with the modified histopathological classification of the American Heart Association (AHA) (Table 2)[64,65]. In the classification introduced here, normal artery and intimal thickening (type I, AHA) observed in conventional histology were combined into normal endoluminal surface in the multimodal SFE. The multimodal SFE does not allow identification of individual cells and therefore is limited to differentiating minor proliferations of smooth muscle cells in a proteoglycan rich matrix and a healthy intima. Intimal xanthomata (type II, AHA), pathologic intimal thickening (type III, AHA), and fibroatheroma (type IV and V, AHA) corresponded to early, intermediate, and advanced lesions per endoscopy, respectively. Complicated plaques (type VI, AHA) include lesions with surface defects (ulcer, erosion, and fissure), intraplaque hemorrhage, and intraluminal thrombus, and corresponded to ulcerated plaque, hemorrhagic plaque, and intraluminal thrombus per endoscopy, respectively. Arterial erosion, which is suspected when a thrombosed arterial segment fails to reveal a fibrous cap rupture in serial histological sectioning and is occasionally encountered in coronary artery disease, was not identified in our carotid sample and therefore not included in the endoscopic classification[20].

In order to define topographic coordinates of endovascular surfaces to facilitate comparisons of different endoscopic systems and match histology sections, we organized the specimens as follows (Supplementary Fig. 4a–c): 1) **Radially.** Using a cross-section of the vessel, we

combined a simplified polar coordinate system (the reference point or pole was considered the center of the image and equidistant rings from the pole to the periphery were numbered from 1 to 6) with a clock face localization system (orientation was given by assigning the origin of ICA at hour 3, and the origin of the ECA at hour 9); 2) **Longitudinally.** Along the main axis of the vessel, the reference point (distance 0) was set at the CB by assigning positive (+) distance values toward the CCA or negative (−) distance values toward the ECA or ICA. Images were obtained via SFE probe introduced into an outer sheath (2ml pipette cut open at 0) labeled with a metric ruler (0cm was considered the distal opening of the sheath where the SFE emerged inside the vessel). This provided the distance from the proximal arterial opening to the SFE tip. This information was then used to match the region of interest observed with the SFE on the external surface of the vessel. In addition, the laser used to excite the endoluminal surfaces during imaging acquisition partially transilluminated the vascular wall that allowed an estimation of the vascular segment being scanned (Fig. 2).

Histological analysis

After endoluminal endoscopy, multiple 5mm segments were cut from each specimen. Arteries with homogeneous unremarkable endoluminal surfaces were serially sectioned at the level of the CB (0cm) and at +1cm, +3cm and +5cm (from the CB toward the CCA), and at −1cm (from the CB toward the ECA and ICA) (Supplementary Fig. 4d). Endoluminal lesions identified during SFA were topographically located on the external surface of the specimens and 1cm vascular segments were harvested. In some cases, multiple lesions at different stages (especially early and intermediate) were identified in the specimens. Despite the possibility of incurring selection bias, in such cases we elected to select only a small subset of lesions that, given their location or relatively normal background, would have facilitated a truthful matching with histopathology. Vessels were then fixed in 10% neutral buffered formalin for 12 hrs at 4 °C, decalcified if needed in buffered ethylenediaminetetraacetic acid (EDTA) for 3–5 days, and embedded in paraffin. Sections were obtained (5μm and 10μm thick) and stained with: (1) hematoxylin and eosin (H&E) for assessment of overall arterial and plaque histology; (2) Movat's pentachrome stain to highlight the various constituents of connective tissue (nuclei and elastic fibers are black; collagen and reticular fibers are yellow; connective ground substance and mucin are blue; fibrin is bright red; and smooth muscle cytoplasm is red); and (3) CD68 immunostaining for plaque macrophage content (CD68 mouse monoclonal antibody, cat# M0814; Dako North America, Inc. Carpinteria, CA). Histology slides were independently evaluated by two pathologists unaware of the patient's medical history and the *ex vivo* endoscopic findings, and lesions were categorized according to a modified AHA histopathological classification (Table 2)[4,20,64,65]. Consensus was reached in cases of initial diagnosis disagreement. Non-stained sections of each vascular segment of interest were imaged with confocal microscopy (Leica SP5X Inverted 2-Photon FLIM Confocal, laser setting equivalent to blue, green, and red laser wavelengths of the SFE system) and AF images obtained. Then, weighted Kappa statistics were calculated to test agreement between the multimodal SFE diagnosis and the pathology diagnosis using conventional histological techniques (Supplementary Table 3). Kappa statistics ranged from 0 (no agreement) to 1 (complete agreement). Significance is determined at $P<0.05$.

Molecular imaging of endarterectomy specimens

Fresh resected plaques were spectrally analyzed using an *in vivo* imaging system (IVIS Spectrum; PerkinElmer, Inc.) and with each channel of the SFE as described above. Then, specimens were incubated in 4nmol of the activatable fluorescence imaging agent MMPSense 645 FAST (PerkinElmer, Inc.) solution diluted in 100μL PBS for 2 hrs at 37 °C, and re-scanned with the IVIS and SFE systems. Then, full-mount fresh specimens were analyzed with an upright Olympus Confocal Microscope using the same excitation wavelength as the SFE red laser, and images were obtained. Fluorescence emission was collected with a fiber-coupled spectrophotometer (Ocean Optics) using a diode-pumped solid state laser with λex = 642nm. The spectra were plotted with GraphPad Prism software (Graphpad Software, Inc.).

In-situ zymography

In order to confirm the presence of active MMP in regions with red fluorescence signal localized by the SFE after MMPSense exposure, *in situ* zymography of corresponding areas was performed. To this end, 10μm thick cryosections of non-fixed endarterectomy specimens were obtained and incubated with DQ™-gelatin (EnzCheck Gelatinase/ Collagenase Assay Kit; Thermo Fisher Scientific, Waltham, MA) for 2hrs at 37 °C, nuclei counterstained with DAPI, and sections analyzed with confocal microscopy as described above. DQ™-gelatin is heavily labeled with fluorescein and releases green fluorescent peptides when enzymatically cleaved. To control for intrinsic tissue AF, a serial section was incubated with 1x PBS for 2 hrs at 37 °C, and nuclei counterstained with DAPI to show cellular components in fluorescence regions that seemed to have no tissue background.

In vivo angioscopy

In vivo endovascular endoscopy of the infrarenal aortoiliac vessels was performed in two New Zealand rabbits with a 1.2mm SFA (Fig. 6 and Supplementary Video 6). In detail, the animals were anesthetized with propofol and ketamine and placed supine on the operating table and the ventral neck shaved and disinfected in usual fashion. Then, a 3cm midline incision was performed in the central neck using blunt dissection techniques, and the right common carotid artery was exposed. Using the reverse Seldinger technique, the right common carotid artery was accessed and a 7F sheath placed and connected to continuous heparinized saline solution (1000μ/mL, ~150units/kg) (Fig. 6a–c). Contrast dye was then hand injected (2mL) over a 2-second period to obtain a control angiogram of the aorta and both iliac arteries. Using fluoroscopic guidance, a 6F+ balloon guide catheter was then advanced into the abdominal aorta using a standard clinical monorail technique. At this point, the SFA was advanced in coaxial fashion and a clear FOV was obtained by anterograde blood flow interruption via balloon insufflation and heparinized normal saline flush[37]. Then, manual advancements/pullbacks of the SFE were performed and multimodal images generated in reflectance and fluorescence modes. At the conclusion of angioscopy, euthanasia was performed and the aortoiliac bifurcation harvested for histological analysis. All experiments involving animals were approved by the Institutional Animal Care and Use Committee of the University of Michigan (protocol number PRO00006157).

Supplementary Material

Refer to Web version on PubMed Central for supplementary material.

Acknowledgments

References

1. Estol CJ. Dr. C. Miller Fisher and the history of carotid artery disease. Stroke. 1996; 27:559–566. [PubMed: 8610329]

2. North American Symptomatic Carotid Endarterectomy Trial Collaborators (NASCET). Beneficial effect of carotid endarterectomy in symptomatic patients with high-grade carotid stenosis. N Engl J Med. 1991; 325:445–453. [PubMed: 1852179]

3. Boyle JJ. Macrophage activation in atherosclerosis: pathogenesis and pharmacology of plaque rupture. Curr Vasc Pharmacol. 2005; 3:63–68. [PubMed: 15638783]

4. Howard DP, et al. Symptomatic carotid atherosclerotic disease: correlations between plaque composition and ipsilateral stroke risk. Stroke. 2015; 46:182–189. [PubMed: 25477221]

5. Ross R. Atherosclerosis--an inflammatory disease. N Engl J Med. 1999; 340:115–126. [PubMed: 9887164]

6. Falk E, Shah PK, Fuster V. Coronary plaque disruption. Circulation. 1995; 92:657–671. [PubMed: 7634481]

7. Fisher M, et al. Carotid plaque pathology: thrombosis, ulceration, and stroke pathogenesis. Stroke. 2005; 36:253–257. [PubMed: 15653581]

8. Sloop GD. Atherosclerosis--an inflammatory disease. N Engl J Med. 1999; 340:1928–1929.

9. Brinjikji W, et al. Contemporary carotid imaging: from degree of stenosis to plaque vulnerability. J Neurosurg. 2016; 124:27–42. [PubMed: 26230478]

10. Edwards JH, Kricheff II, Riles T, Imparato A. Angiographically undetected ulceration of the carotid bifurcation as a cause of embolic stroke. Radiology. 1979; 132:369–373. [PubMed: 461794]

11. Saam T, et al. The vulnerable, or high-risk, atherosclerotic plaque: noninvasive MR imaging for characterization and assessment. Radiology. 2007; 244:64–77. [PubMed: 17581895]

12. ten Kate GL, et al. Noninvasive imaging of the vulnerable atherosclerotic plaque. Curr Probl Cardiol. 2010; 35:556–591. [PubMed: 20974314]

13. Mulder WJ, Jaffer FA, Fayad ZA, Nahrendorf M. Imaging and nanomedicine in inflammatory atherosclerosis. Sci Transl Med. 2014; 6:3005101.

14. Sanz J, Fayad ZA. Imaging of atherosclerotic cardiovascular disease. Nature. 2008; 451:953–957. [PubMed: 18288186]

15. Lee CM, et al. Scanning fiber endoscopy with highly flexible, 1 mm catheterscopes for wide-field, full-color imaging. J Biophotonics. 2010; 3:385–407. [PubMed: 20336702]

16. Tarkin JM, Joshi FR, Rudd JH. PET imaging of inflammation in atherosclerosis. Nat Rev Cardiol. 2014; 11:443–457. [PubMed: 24913061]

17. Krejza J, et al. Carotid artery diameter in men and women and the relation to body and neck size. Stroke. 2006; 37:1103–1105. [PubMed: 16497983]

18. Lenglet S, et al. Molecular imaging of matrix metalloproteinases in atherosclerotic plaques. Thromb Haemost. 2012; 107:409–416. [PubMed: 22274652]

19. Tarkin JM, et al. Imaging atherosclerosis. Circ Res. 2016; 118:750–769. [PubMed: 26892971]

20. Virmani R, Ladich ER, Burke AP, Kolodgie FD. Histopathology of carotid atherosclerotic disease. Neurosurgery. 2006; 59:S3–13.

21. Ishibashi F, Aziz K, Abela GS, Waxman S. Update on coronary angioscopy: review of a 20-year experience and potential application for detection of vulnerable plaque. J Interv Cardiol. 2006; 19:17–25. [PubMed: 16483335]

22. Mizuno, K., Takano, M. Coronary Angioscopy. Springer; Tokyo: 2015.

23. Tanemura H, et al. Angioscopic observation during carotid angioplasty with stent placement. AJNR Am J Neuroradiol. 2005; 26:1943–1948. [PubMed: 16155139]

24. Uchida, Y. Coronary Angioscopy. Wiley; Armonk, NY: 2001.

25. White JV, Eid I. Diagnostic and interventional angioscopy. Surg Clin North Am. 1998; 78:539–559. [PubMed: 9728200]

26. Uchida Y, et al. Detection of vulnerable coronary plaques by color fluorescent angioscopy. JACC Cardiovasc Imaging. 2010; 3:398–408. [PubMed: 20394902]

27. Uchida Y. Recent advances in coronary angioscopy. J Cardiol. 2011; 57:18–30. [PubMed: 21146367]

28. Arakawa K, et al. Fluorescence analysis of biochemical constituents identifies atherosclerotic plaque with a thin fibrous cap. Arterioscler Thromb Vasc Biol. 2002; 22:1002–1007. [PubMed: 12067911]

29. Marcu L, et al. Detection of rupture-prone atherosclerotic plaques by time-resolved laser-induced fluorescence spectroscopy. Atherosclerosis. 2009; 204:156–164. [PubMed: 18926540]

30. Bartorelli AL, et al. In vivo human atherosclerotic plaque recognition by laser-excited fluorescence spectroscopy. J Am Coll Cardiol. 1991; 17:160B–168B.

31. Otsuka F, et al. Clinical classification of plaque morphology in coronary disease. Nat Rev Cardiol. 2014; 11:379–389. [PubMed: 24776706]

32. Tearney GJ, et al. Three-dimensional coronary artery microscopy by intracoronary optical frequency domain imaging. JACC Cardiovasc Imaging. 2008; 1:752–761. [PubMed: 19356512]

33. van Soest G, et al. Pitfalls in plaque characterization by OCT: image artifacts in native coronary arteries. JACC Cardiovasc Imaging. 2011; 4:810–813. [PubMed: 21757174]

34. Farooq V, et al. New insights into the coronary artery bifurcation hypothesis-generating concepts utilizing 3-dimensional optical frequency domain imaging. JACC Cardiovasc Interv. 2011; 4:921–931. [PubMed: 21851908]

35. Okamura T, Fujimura T, Yano M. Three-dimensional reconstruction of optical coherence tomography for improving bifurcation stenting. J Cardiol Cases. 2016; 13:137–138.

36. Iakovou I, et al. Incidence, predictors, and outcome of thrombosis after successful implantation of drug-eluting stents. JAMA. 2005; 293:2126–2130. [PubMed: 15870416]

37. McVeigh PZ, et al. High-resolution angioscopic imaging during endovascular neurosurgery. Neurosurgery. 2014; 75:171–180. [PubMed: 24762703]

38. Wiethoff A, et al. Molecular imaging of thrombosis. Curr Cardiovasc Imaging Rep. 2010; 3:34–41.

39. Bang OY, et al. Frequency and mechanisms of stroke recurrence after cryptogenic stroke. Ann Neurol. 2003; 54:227–234. [PubMed: 12891675]

40. Joshi BP, et al. Multispectral endoscopic imaging of colorectal dysplasia in vivo. Gastroenterology. 2012; 143:1435–1437. [PubMed: 23041325]

41. Finn AV, et al. Concept of vulnerable/unstable plaque. Arterioscler Thromb Vasc Biol. 2010; 30:1282–1292. [PubMed: 20554950]

42. Newby AC. Metalloproteinases and vulnerable atherosclerotic plaques. Trends Cardiovasc Med. 2007; 17:253–258. [PubMed: 18021934]

43. Bourantas CV, et al. Hybrid intravascular imaging: recent advances, technical considerations, and current applications in the study of plaque pathophysiology. Eur Heart J. 2016 Apr 26. Epub ahead of print.

44. Jaffer, FA., Libby, P. Molecular imaging of coronary atherosclerosis. In: Nicholls, SJ., editor. Imaging Coronary Atherosclerosis. Springer; New York: 2014. p. 187-202.

45. Ughi GJ, et al. Clinical Characterization of Coronary Atherosclerosis With Dual-Modality OCT and Near-Infrared Autofluorescence Imaging. JACC Cardiovasc Imaging. 2016; 3:00038–00033.

46. Arbab-Zadeh A, Fuster V. The myth of the "vulnerable plaque": transitioning from a focus on individual lesions to atherosclerotic disease burden for coronary artery disease risk assessment. J Am Coll Cardiol. 2015; 65:846–855. [PubMed: 25601032]

47. Kim DE, et al. Protease imaging of human atheromata captures molecular information of atherosclerosis, complementing anatomic imaging. Arterioscler Thromb Vasc Biol. 2010; 30:449–456. [PubMed: 20056915]

48. Kataiwa H, et al. Safety and usefulness of non-occlusion image acquisition technique for optical coherence tomography. Circ J. 2008; 72:1536–1537. [PubMed: 18724035]

49. Biamino G. The excimer laser: science fiction fantasy or practical tool? J Endovasc Ther. 2004; 11:II207–222. [PubMed: 15760264]

50. Abela GS, et al. Laser recanalization of occluded atherosclerotic arteries in vivo and in vitro. Circulation. 1985; 71:403–411. [PubMed: 3965181]

51. Karsch, KR., Haase, KK. Coronary Laser Angioplasty: An Update. Springer-Verlag; Berlin: 1991.

52. Leon MB, et al. Human arterial surface fluorescence: atherosclerotic plaque identification and effects of laser atheroma ablation. J Am Coll Cardiol. 1988; 12:94–102. [PubMed: 3379220]

53. Kirshenbaum, MR., Seibel, EJ. Delivery of single-mode and multi-mode therapeutic laser light using a single and dual cladding optical fiber for a scanning fiber endoscope. Proc. SPIE7894, Optical Fibers, Sensors, and Devices for Biomedical Diagnostics and Treatment XI; San Francisco. February 16, 2011;

54. Woldetensae, MH., et al. Fluorescence image-guided photodynamic therapy of cancer cells using a scanning fiber endoscope. Proc. SPIE 8576, Optical Fibers and Sensors for Medical Diagnostics and Treatment Applications XIII; San Francisco. March 20, 2013;

55. Deckelbaum, LI. Laser-induced arterial fluorescence spectroscopy. In: Abela, GS., editor. Lasers in Cardiovascular Medicine and Surgery: Fundamentals and Techniques. Kluwer; Boston: 1990. p. 153-165.

56. Dippel EJ, et al. Randomized controlled study of excimer laser atherectomy for treatment of femoropopliteal in-stent restenosis: initial results from the EXCITE ISR trial (EXCImer Laser Randomized Controlled Study for Treatment of FemoropopliTEal In-Stent Restenosis). JACC Cardiovasc Interv. 2015; 8:92–101. [PubMed: 25499305]

57. Fifi JT, et al. Complications of modern diagnostic cerebral angiography in an academic medical center. J Vasc Interv Radiol. 2009; 20:442–447. [PubMed: 19246211]

58. Crouse JR, et al. Risk factors for extracranial carotid artery atherosclerosis. Stroke. 1987; 18:990–996. [PubMed: 3686596]

59. Yang C, et al. Target-to-background enhancement in multispectral endoscopy with background autofluorescence mitigation for quantitative molecular imaging. J Biomed Opt. 2014; 19:076014.

60. Zhang L, et al. Trimodal detection of early childhood caries using laser light scanning and fluorescence spectroscopy: clinical prototype. J Biomed Opt. 2013; 18:111412. [PubMed: 23986369]

61. Yang C, Hou V, Nelson LY, Seibel EJ. Color-matched and fluorescence-labeled esophagus phantom and its applications. J Biomed Opt. 2013; 18:026020.

62. Wang TD, et al. Mathematical model of fluorescence endoscopic image formation. Appl Opt. 1998; 37:8103–8111. [PubMed: 18301704]

63. Savastano L, et al. Diagnostic and interventional optical angioscopy in ex vivo carotid arteries. Neurosurgery. 2016 Aug. 1 accepted for publication.

64. Stary H, et al. A definition of advanced types of atherosclerotic lesions and a histological classification of atherosclerosis. A report from the Committee on Vascular Lesions of the Council on Arteriosclerosis, American Heart Association. Circulation. 1995; 92:1355–1374. [PubMed: 7648691]

65. Virmani R, et al. Lessons from sudden coronary death: a comprehensive morphological classification scheme for atherosclerotic lesions. Arterioscler Thromb Vasc Biol. 2000; 20:1262–1275. [PubMed: 10807742]
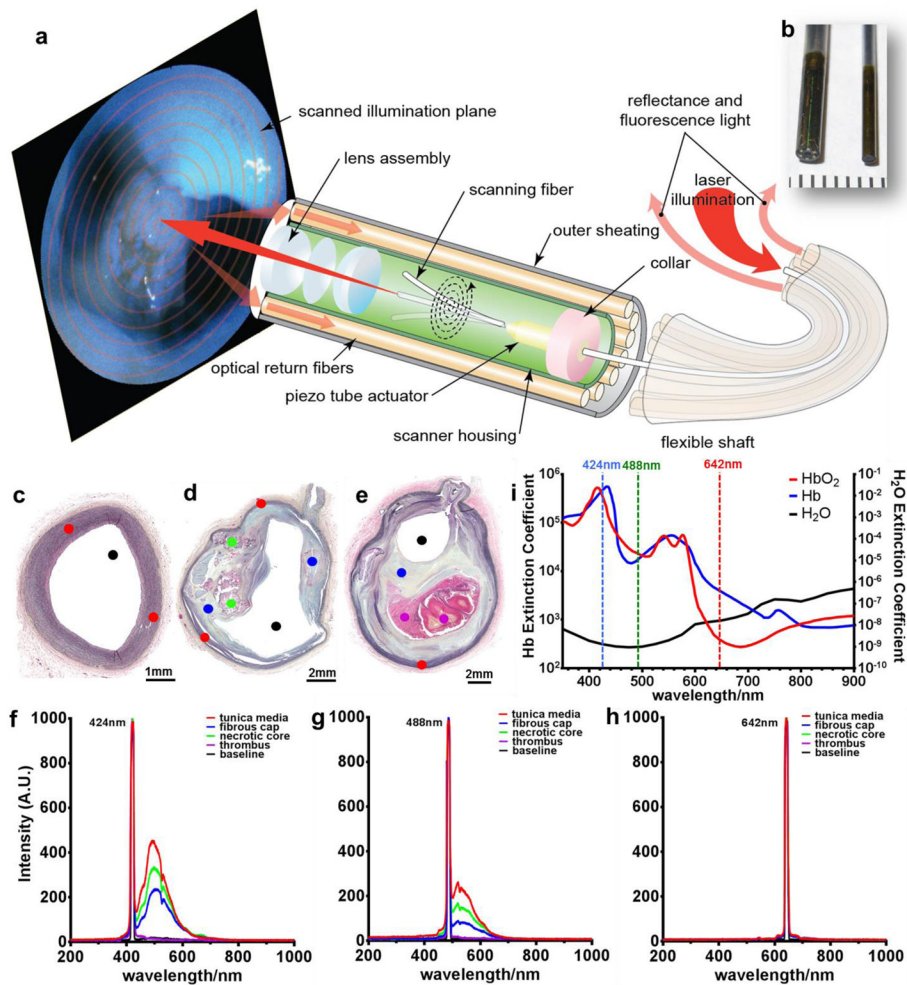
Figure 1. Scanning fiber endoscope optics and fluorescence spectrometry of major structural constituents of atherosclerotic plaques

a, The scanning fiber endoscope excites tissues by scanning blue (424nm), green (488nm) and red lasers (642nm) in a spiral pattern. Backscattered (reflectance) light and fluorescent signal is collected by a ring of optical fibers located in the periphery of the scanner housing and shaft, and conducted to a computer for image generation. **b,** The optical system can be mounted in 2.1mm (left) or 1.2mm (right) endoscopes. **c–h,** Fluorescence spectrometry of representative samples of histology-proven tunica media (red dot), fibrous cap (blue dot), necrotic core (green dot), and thrombus (fuchsia dot) were collected with a fiber-coupled spectrophotometer from **(c)** normal arterial walls, **(d)** fibroatheroma, and **(e)** ruptured plaque with associated thrombus after excitation with scanning fiber endoscope lasers [**(f)** λex=424nm; **(g)** 488nm; **(h)** 642nm]. **i,** By spreading out the excitation wavelengths of the 3 lasers over the visible and near-infrared spectrum of light, multimodal scanning fiber endoscopy has the capability to excite tissue autofluorescence for spectral biochemical analysis and provide a broad, non-overlapping range of colors for multiplexed molecular images. **h,** Molecular probes labeled with red dyes are particularly convenient for endovascular use, based on the negligible autofluorescence excited at 642nm that enables higher target-to-background ratios. **i,** In addition, the extinction coefficient of hemoglobin

(Hb) is greatly reduced in the red and near-infra red spectrum, which translates into lower attenuation of fluorescence signal through tissue and blood. On the opposite end of the visible spectrum, the extinction coefficient of hemoglobin (Hb) is at its peak, which translates into high absorption at 424nm. The hemoglobin-related light extinction results in a void in autofluorescence detection, turning hemoglobin into a physiological negative contrast in spectral imaging.
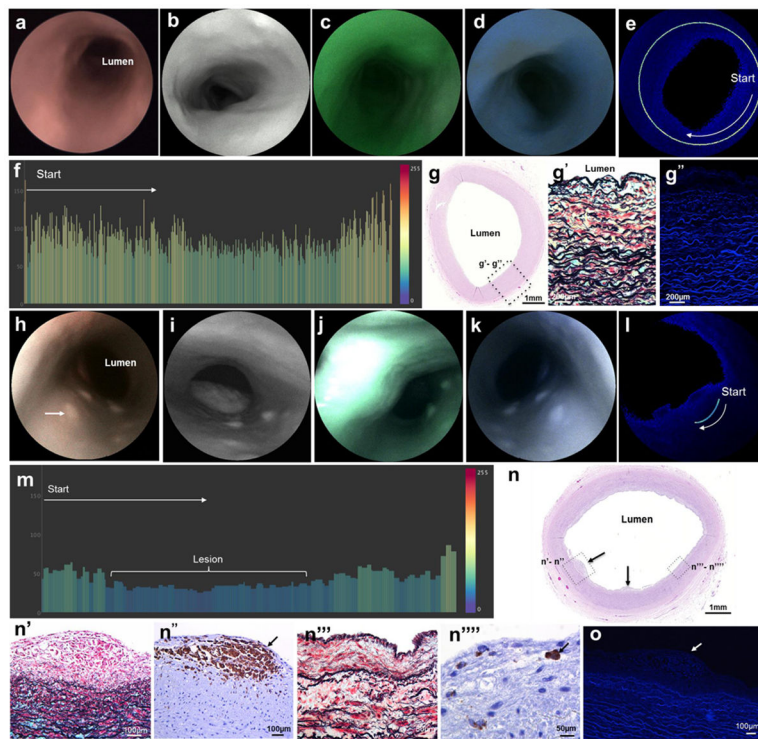
Figure 2. Multimodal endoluminal scanning fiber angiography of (a–h) normal carotid artery and (i–p) early lesion

b&i, White-light endoscopic system images. **c&j,** Scanning fiber endoscopy images with red reflectance. **d&k,** Scanning fiber endoscopy images with red reflectance and laser-induced green fluorescence. **f&m,** Post-acquisition processing allows isolation of fluorescence signal by extracting light reflectance and correcting the distance from tissue to scanning fiber endoscope tip. **g&n,** Bar charts are created by plotting the color-coded pixel values of every dot of a line traced in the endoscopic images. Pixel values range from 0 to 255. **a,** Dotted line represents scanning fiber endoscope entering common carotid artery toward bifurcation. **b–f, Normal Artery**: Delicate smooth endoluminal surfaces with homogeneous reflectance, absent red fluorescence, and intense green and blue autofluorescence. **h&h¹,** hematoxylin and eosin-stained vessel cross-section shows normal arterial wall, and under higher magnification it is possible to identify healthy tunica intima (TI), tunica media (TM), and tunica externa/adventitia (TE). **h²,** Note the robust internal elastic membranes (black wavy lines) very close to the vascular lumen and the wavy elastic fibers in the tunica media in the pentachrome-stained slide, intermixed with a collagen matrix and smooth muscle cells (yellow and red stained, respectively). **h³,** Confocal microscopy of the same vascular section revealed very strong blue and green autofluorescence originating from the elastin, with gentle autofluorescence background from the collagen matrix. **i–m, Early Lesion:** Note the small elevated lesion (arrow) facing the lumen of the internal carotid artery with preserved reflectance but decreased autofluorescence, better appreciated in the distance-compensated fluorescence image. **n,** Color-coded bar chart of pixel values of a line traced in **(m)** reveals drop of 10–20 points of autofluorescence registered from the lesion in comparison to surrounding vascular surface. **o,** Histological analysis of artery cross-section reveals multiple small elevated focal intimal

lesions (arrows). **o^1&o^2,** Under higher magnification, it is possible to appreciate focal accumulations of fat-laden macrophages (arrow) corresponding to a fatty streak lesion (Grade II intimal xanthoma). **o^3&o^4,** An adjacent area shows a thickened intima rich in smooth muscle cells and occasional macrophages (arrow) corresponding to intima thickening (Grade I). **o^1&o^3,** Movat's pentachrome stain. **o^2&o^4,** CD68 immunostain. **p,** Confocal microscopy of same vascular section revealed lower autofluorescence from thickened intima and early plaque with fat-laden macrophages (arrow) in comparison with the intense signal from elastin in the tunica media.
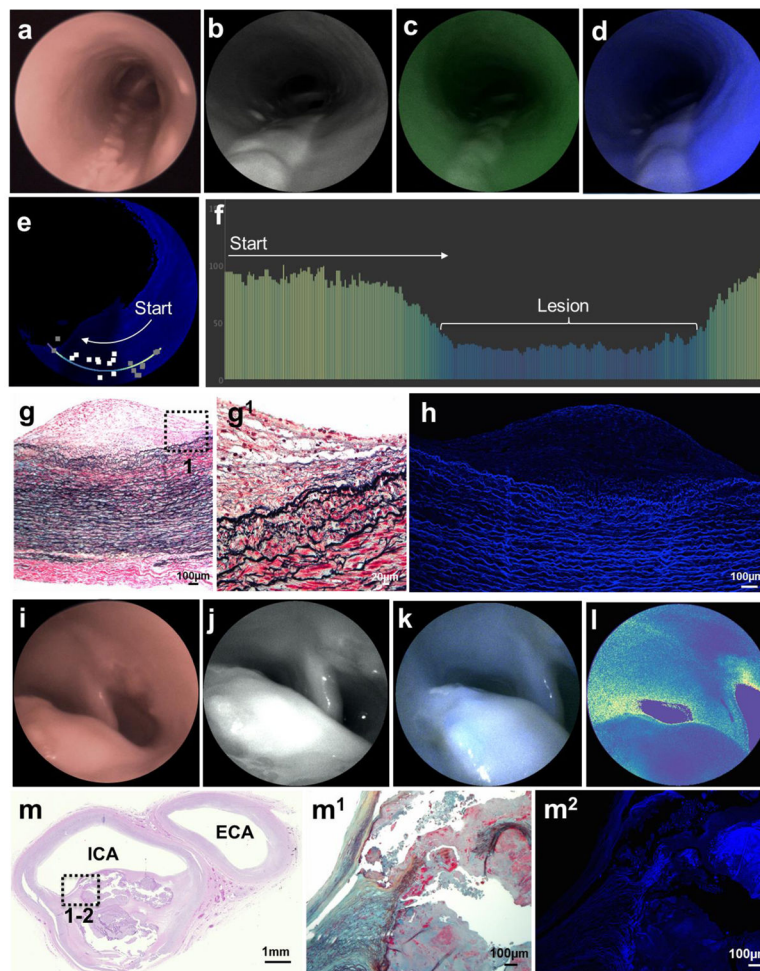
Figure 3. Multimodal endovascular scanning fiber angiography of (a–h) intermediate and (i–m) advanced lesions

a&i, White-light endoscopic system images. **b&j,** Scanning fiber endoscopy images with red reflectance. c, Scanning fiber endoscopy images with red reflectance and laser-induced green fluorescence. **d&k,** Scanning fiber endoscopy images with red reflectance and laser-induced blue fluorescence. e, Distance-compensated fluorescence image. **a–e, Intermediate Lesion**: Note the large longitudinal elevated lesions with loss of blue and green autofluorescence, which is better appreciated in the distance-compensated fluorescence image. Note the 10 random square areas in lesion and 10 in background used for target-to-background ratio. **f,** Color-coded bar chart of pixel values of a line traced in (**e**) reveals >50 points drop of autofluorescence intensity registered from the lesion in comparison to surrounding vascular background, on average 2.5 times stronger. **g,** Histological analysis of arterial cross-section reveals multiple layers of fat-laden macrophages at the intima with sparse free-lipid deposits in deep portion of the lesion (Movat's stain). This is a Grade III intermediate lesion. **g^1,** Higher magnification of the plaque shoulder [dotted box in (**g**)] shows no distinct necrotic core. **h,** Confocal microscopy revealed very low autofluorescence derived from the intermediate atheroma, compared to the intense autofluorescence originating from elastin in the tunica media. **i–l, Advanced Lesion**: Protruding lesion with

smooth homogeneous surface in carotid bifurcation causing significant luminal stenosis. **l,** This lesion is associated with low autofluorescence, which is better appreciated in distance-compensated pseudocolor map. **m,** Histological analysis of arterial cross-section reveals a fibroatheroma (Grade IV) extending from carotid bifurcation into proximal internal carotid artery [**(m)** hematoxylin and eosin stain, with dotted insert represented in **(m^1)**, Movat's pentachrome stain]. **m^2,** Confocal microscopy shows a poorly fluorescent collagenous fibrous cap overlying a necrotic core with heterogeneous fluorescence.
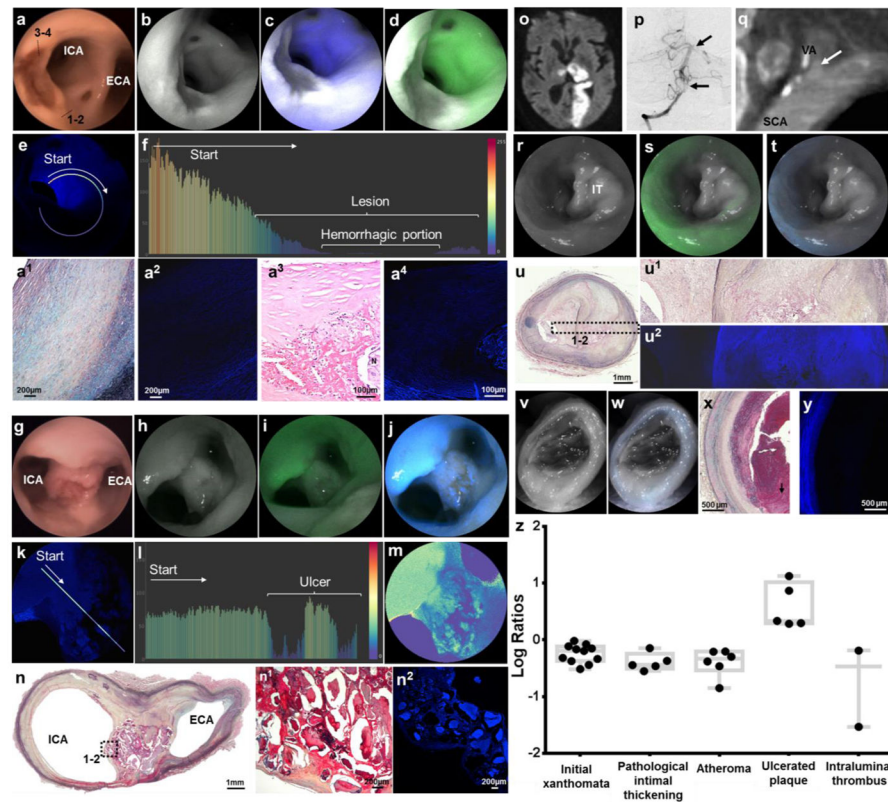
Figure 4. Multimodal endovascular SFA of complicated plaques

a–e, Intraplaque Hemorrhage: Large elevated lesions associated with very poor blue and green autofluorescence, better appreciated in distance-compensated fluorescence image. Note the distinct reddish-brown central portion on white light, corresponding to the very low reflectance area (dark grey area, **b–d**). **f,** Color-coded bar chart of pixel values of a line traced in (e) reveals >200-point drop of autofluorescence signal down to undetectable levels in the hemorrhagic component. $\mathbf{a^1}$, Histological analysis of the plaque portion with preserved reflectance and decreased autofluorescence [dotted line, **area 1–2 in (a)**] reveals a thick layer of smooth muscle cells in a collagenous proteoglycan matrix covering a lipid or necrotic core consistent with a fibrotic atheroma (Grade IV, Movat's stain). $\mathbf{a^2}$, Confocal microscopy of consecutive tissue section revealed low autofluorescence derived from the fibroatheroma, compared to the intense autofluorescence originating from elastin in the tunica media. $\mathbf{a^3}$, Histological analysis of the plaque portion with low reflectance and autofluorescence [dotted line, **area 3–4 in (a)**] reveals a complex atheroma with recent intraplaque hemorrhage (hematoxylin and eosin stain). $\mathbf{a^4}$, Confocal microscopy of a magnified section of the complex fibroatheroma reveals strong autofluorescence from tunica media, low autofluorescence from fibrotic cap, and negligible autofluorescence from intraplaque hemorrhage forming a black halo around a necrotic core with heterogeneous autofluorescence. **g–n, Ulcerated Plaque**: Punched-out lesion with irregular elevated borders at the carotid bifurcation on **(g)** white-light system, **(h)** red reflectance, and reflectance with **(i)** green and **(j)** blue channels, better appreciated in **(k)** distance-compensated image. Note the speckled pattern in the crater of the ulcer with multiple

irregular dots of strong autofluorescence in a background of very low autofluorescence. **l,** The normalized pixel fluorescence difference is >75 points as demonstrated in color-coded bar chart of the line traced in **(k). m,** The speckled pattern can be better appreciated in pseudocolor image. n, Histological analysis of axial cut at the bifurcation reveals an atherosclerotic plaque (Movat's stain; higher magnification in n^1) with necrotic debris, some of which appears calcified, with (n^2) highly heterogenous autofluorescence signal on confocal microscopy. **o–y, Ruptured Plaque with Intraluminal Thrombus**: Left subclavian artery (SCA) and left vertebral artery (VA) of a man with a large left-sided stroke [(o) brain MRI] secondary to artery-to-artery embolic occlusion of distal left vertebral artery and basilar artery [**(p)** arrows in anteroposterior cerebral angiogram]. **q,** Computed tomographic angiography showed atherosclerotic plaque at origin of the vertebral artery, associated with extensive luminal defect likely caused by thrombus (arrow). At time of autopsy, left subclavian artery and vertebral artery were harvested and multimodal endovascular scanning fiber angiography was performed. **r–t,** A sub-occlusive lesion with preserved reflectance and minimal fluorescence was found to extend distally into vertebral artery. $\mathbf{u\&u^1}$, Histological analysis revealed an organized chronic intraluminal thrombus associated with a complicated plaque [**(u)** Movat's pentachrome, and **(u^1)** high magnification insert], with significant intraplaque vascularization, commonly resulting from organized thrombus/hemorrhage. $\mathbf{u^2,}$ The thrombus has very low autofluorescence on confocal microscopy in comparison with the underlying fibroatheroma. **v–w,** Scanning fiber angiography analysis of distal vertebral artery revealed an occlusive lesion with negligible reflectance and autofluorescence. **x–y,** This corresponded to acute intraluminal thrombus with absent fluorescence signal on confocal microscopy. **z,** In the boxplot ANOVA model for log-transformed fluorescent target-to-background ratio comparison between different pathological diagnoses, all diagnoses had target-to-background ratios <0 except ulcerated plaque.
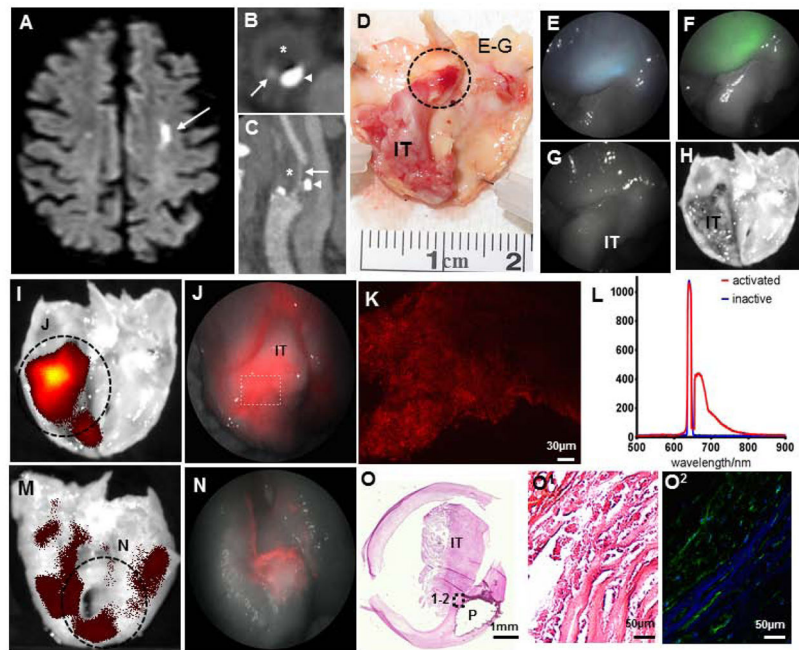
Figure 5. Multimodal endovascular scanning fiber angioscopy of proteolytic activity in endarterectomy specimen

An elderly man suffered a left hemispheric ischemic stroke [(**a**) brain MRI; arrow points to ischemic region] secondary to ipsilateral complicated carotid plaque [(**b**) computed tomographic angiography of axial plane, and (**c**) sagittal reconstruction with arrows pointing to the remaining vascular lumen, arrowheads pointing to calcification, and asterisks indicating fibroatheroma]. **d,** At surgery, the fibroatheroma was removed and found to have a ruptured cap associated with a large intraluminal thrombus. **e–f,** Scanning fiber endoscopy imaging of the region highlighted in (**d**) revealed delicate blue and green autofluorescence originating from the fibrous cap, with preserved reflectance and absent autofluorescence from the intraluminal thrombus. **g,** No fluorescent signal was identified in the reflectance or red channel, which was then confirmed by (**h**) scanning tissue with IVIS. **i,** After incubation with MMPSense, strong signal is observed from the cap surrounding the intraluminal thrombus using IVIS, which is clearly detected by (**j**) scanning fiber angioscopy with high spatial resolution. Note the geographic and intensity differences of specific red signals obtained from the (**i–j**) endoluminal surface in comparison with (**m–n**) the abluminal surface of the plaque. **k**, Red signal detected with scanning fiber angioscopy from activation of the molecular probe was confirmed with upright confocal microscopy in fresh full-mount specimen. **l,** Point-spectrometer revealed a maximum fluorescence emission of 666nm for activated MMPSense 645, and inactive MMPSense 645 was optically silent. **o,** Histological analysis of the specimen revealed a large intraluminal thrombus with an underlying complicated fibroatheroma. **p**, *In situ* zymography of the fibrous cap underlying the thrombus with (**q**) DQ-gelatin-confirmed high gelatinase activity from matrix metalloproteinases.
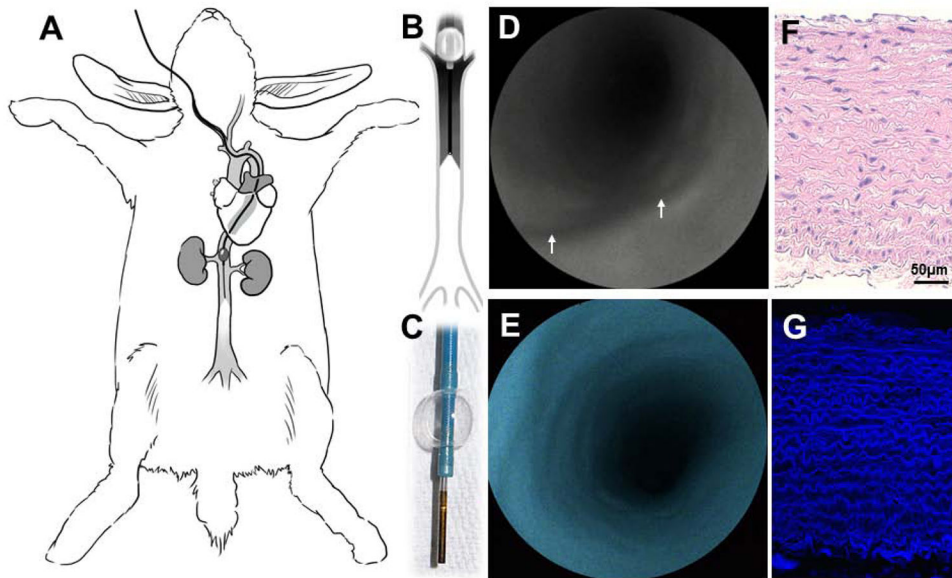
Figure 6. *In vivo* **angioscopy in rabbit**
a, Under roadmap angiography of rabbit aorta, **(b–d)** a 6F+ balloon guide catheter is navigated from a carotid artery into the infrarenal aorta and a 1.2mm scanning fiber endoscope is introduced in coaxial fashion. **e–f,** After balloon insufflation and saline flush, high-definition multimodal angioscopy can be obtained. Note the smooth surface in the aorta with reflection (arrows in **(e)** point to ostia of arterial branches emerging from the aorta) and **(f)** homogeneous blue autofluorescence. **g,** Histological analysis shows a healthy arterial wall mainly formed by tunica media (hematoxylin and eosin stain, with **(h)** intense autofluorescence from elastin by confocal microscopy.

Table 1

Laser-induced peak intensities of representative samples of histology-proven tunica media, fibrous cap, necrotic core, and thrombus. Peak intensities were collected with a fiber-coupled spectrophotometer from normal arterial walls, fibroatheroma, and ruptured plaque with associated thrombus after excitation with SFE lasers (λex = 424nm, 488nm and 642nm).

Channel	Tunica Media	Fibrous Cap	Necrotic Core	Thrombus	Baseline	Emission Peak
424	453.7	237.8	336.3	16.2	19.7	482nm
488	262.0	89.6	167.6	20.1	14.4	510nm
642	31.0	24.1	30.3	28.6	9.7	649nm

Table 2

Comparison of American Heart Association's histopathological classification[20,64,65] and proposed endovascular SFA classification of atherosclerosis.

Atherosclerosis Grade	Modified AHA Classification	Histology findings	Endovascular SFA Classification	Endoluminal description
Normal artery	Normal artery	Three concentrically oriented layers: 1) TI formed by endothelium overlying a thin connective tissue with a prominent internal elastic membrane; 2) TM with abundant smooth muscle cells in a wavy matrix of elastic fibers and collagen; 3) TE with collagen fibers and fibroblasts.	Normal endoluminal surface	Delicate smooth endoluminal surfaces with homogeneous reflectance, blue and green AF.
Grade I	Intimal thickening	Proliferation of smooth muscle cells underlying the intima, in a proteoglycan-rich matrix. It does not contain macrophages.	Early lesion	Slightly raised, small dot-like or streak-like endoluminal lesions with preserved reflectance and slightly lower AF in blue and green channels compared to surrounding surface.
Grade II	Intimal xanthomata	Focal accumulations of fat-laden macrophages at the intima. Predominantly contain macrophages and few T-cells and smooth muscle cells.		
Grade III	Pathologic intimal thickening or intermediate lesion	True necrosis is not apparent, and there is no evidence of cellular debris; some lipid may be present deep in the lesion, but it is dispersed. The fibrous cap overlying the areas of lipid is rich in smooth muscle cells and proteoglycans. Some scattered macrophages and lymphocytes may also be present, but these are usually sparse.	Intermediate lesion	Longitudinal elevated lesions with preserved reflectance and low blue and green AF compared to surrounding surface.
Grade IV	Fibrous cap atheroma	Thick layer of connective tissue covering the lipid or necrotic core. The cap consists purely of smooth muscle cells in a collagenous proteoglycan matrix, with varying degrees of infiltration by macrophages and lymphocytes.	Advanced lesion	Large lesions protruding into the lumen or causing circumferential stenosis. Lesions have smooth homogeneous surfaces with preserved reflectance, with reduction of luminal AF proportional to the thickness of the fibrous cap.
Grade V	Thin fibrous cap atheroma	Thin fibrous cap (mean cap thickness of 74μm±24μm) heavily infiltrated by macrophages with loss of smooth muscle cells, overlying a large necrotic core (approximately 25% of plaque area).		
Grade VI	Complicated plaque	Surface defects include: • Ulcer: excavation in the endoluminal surface of a plaque caused by embolization of thrombus with a portion of the necrotic core after exposure to lumen surface; • Erosion: identified when serial sectioning of a thrombosed arterial segment fails to reveal fibrous cap rupture. Typically, the endothelium is absent at the erosion site. The exposed intima consists predominantly of smooth muscle cells and proteoglycans,	Ulcerated plaque	Ulcers appear as punched-out lesions with slightly raised, irregular bead-like borders and a central dark grey crater with reflectance and "starry sky" speckled pattern in blue and green channels.

Atherosclerosis Grade	Modified AHA Classification	Histology findings	Endovascular SFA Classification	Endoluminal description
		and surprisingly, the eroded site contains minimal inflammation; • Fissure or rupture: clear communication between the lipid core and the lumen with a break in the fibrous cap.		
		Intraplaque hemorrhage is an area of the plaque with fresh or organized erythrocytes causing disruption of plaque architecture.	**Hemorrhagic plaque**	Distinct dark grey area in the dome of plaques with low reflectance and negligible AF.
		Thrombus is a mass formed by erythrocytes, fibrin, and platelets in the luminal side of a plaque.	**Plaque with intraluminal thrombus**	Occlusive or sub-occlusive intraluminal lesion with variable reflectance (preserved in chronic clots and diminished in acute clots) and negligible AF.